

Event Camera Data Dense Pre-training

Yan Yang¹ Liyuan Pan² Liu Liu³

¹BDSI, ANU ²BITSZ & School of CSAT, BIT ³KooMap Dept., Huawei

Yan.Yang@anu.edu.au liyuan.pan@bit.edu.cn liuliu33@huawei.com

Abstract

This paper introduces a self-supervised learning framework designed for pre-training neural networks tailored to dense prediction tasks using event camera data. Our approach utilizes solely event data for training.

Transferring achievements from dense RGB pre-training directly to event camera data yields subpar performance. This is attributed to the spatial sparsity inherent in an event image (converted from event data), where many pixels do not contain information. To mitigate this sparsity issue, we encode an event image into event patch features, automatically mine contextual similarity relationships among patches, group the patch features into distinctive contexts, and enforce context-to-context similarities to learn discriminative event features.

For training our framework, we curate a synthetic event camera dataset featuring diverse scene and motion patterns. Transfer learning performance on downstream dense prediction tasks illustrates the superiority of our method over state-of-the-art approaches. Notably, our single model secured the top position in the challenging DSEC-Flow benchmark.

1. Introduction

An event camera asynchronously records pixel-wise brightness changes of a scene [18]. In contrast to conventional RGB cameras that capture all pixel intensities at a fixed frame rate, event cameras offer a high dynamic range, temporal resolution, and robustness to lighting changes and motion blur, showing promising applications in diverse vision tasks [4, 23, 43, 51].

This paper addresses the task of pre-training neural networks with event camera data for dense prediction tasks, including segmentation, depth estimation, and optical flow estimation. Our self-supervised method is pre-trained solely with event camera data. One can simply transfer our pre-trained model for dense prediction tasks. Please refer to Fig. 1 for the performance comparisons.

The direct way to pre-training is supervised training, us-

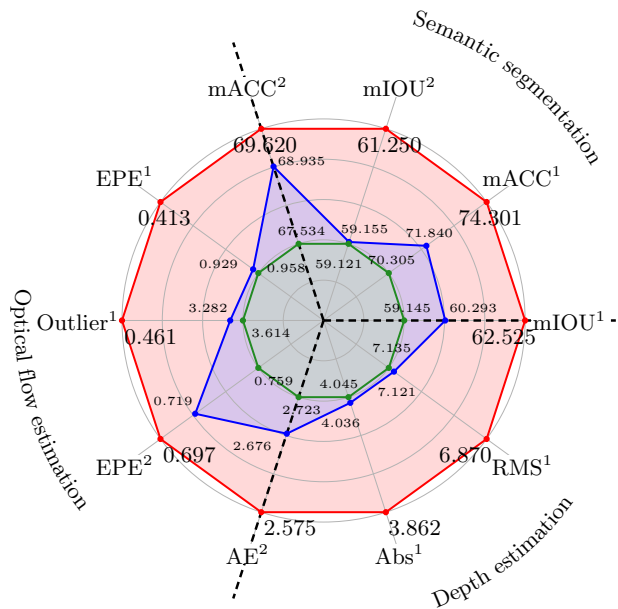


Figure 1. Comparison of *our* scores with respect to the *second-best* and *third-best* scores for semantic segmentation [1, 4, 20, 39], optical flow estimation [20, 21, 51], and depth estimation [51]. Superscripts besides evaluation metrics are used to differentiate benchmark datasets for a specific task.

ing dense annotations for event data. However, due to the scarcity of dense annotations [4, 20, 51], training large-scale networks becomes challenging [12, 15].

An alternative to supervised pre-training is self-supervised learning for event camera data [46, 50], which has been proposed very recently. These approaches necessitate paired RGB images and event data, enforcing image-level embedding similarities between RGB images and event data. This form of RGB-guided pre-training directs networks to focus on the overall structure of events, neglecting intricate pixel-level features that are crucial for dense prediction tasks.

Next to pre-training is transferring the achievements of dense RGB pre-training [27, 42] to event camera data. One may first convert event camera data to an event image [46], split the image into patches, and then learn fine-

grained patch features by enforcing patch-to-patch similarities in a self-supervised learning framework. While feasible, this baseline approach is constrained as event images are sparse, containing patches with little to no information, often from the meaningless background. The sparsity diminishes the discriminativeness of an event patch, introduces background noise/bias to the patch feature learning, and makes training unstable.

Inspired by the above discriminative self-supervised approaches that learn features at the image and patch level, we show that fine-grained event features can be learned by enforcing context-level similarities among patches. Our motivation is described below.

Given an event image, humans can recognize objects (*e.g.*, buildings and trees) by considering multiple similar pixels. In essence, a group of event image pixels contains sufficient information to make them discriminative. Inspired by this insight, we propose to automatically mine the contextual similarity relationship among patches, group patch features into discriminative contexts, and enforce context-to-context similarities. This context-level similarity, requiring no manual annotation, not only promotes stable training but also empowers the model to achieve highly accurate dense predictions.

Our contributions are summarized as follows:

- A self-supervised framework for pre-training a backbone network for event camera dense prediction tasks. The pre-trained model can be transferred to diverse downstream dense prediction tasks;
- Introduction of a context-level similarity loss to address the sparsity issue of event data for learning discriminative event features;
- Construction of a pre-training dataset based on the TartanAir dataset [41], covering diverse scenes and motion patterns to facilitate network training;
- State-of-the-art performance on standard event benchmark datasets for dense prediction tasks.

Moreover, our method ranked first in the online DSEC-Flow benchmark [20, 21]. All codes and pre-trained models will be released.

2. Related Works

We survey recent advancements in self-supervised learning frameworks applied to RGB and event image domains. We then provide an overview of event datasets used for network pre-training and downstream task fine-tuning.

RGB image self-supervised learning. Research in self-supervised learning generally falls into three categories: i) contrastive learning. Images are augmented into multiple views for instance discrimination. By defining a matching pair (*e.g.*, views from the same image), the similarity between them is maximized [8, 22]. Some works also enforce dissimilarity among non-matching pairs [7, 9, 10, 24, 44];

ii) masked image modeling. With unmasked image patches, the networks are trained to reconstruct masked ones. The reconstruction targets can be represented as intensity values of patch pixels [25, 45], discrete indices assigned by an image tokenizer [3, 16, 35], or patch embeddings obtained from pre-trained vision foundation models [17, 36]; iii) self-distillation. This category can be considered as an extension of contrastive learning from instances to groups [5, 6], and is usually combined with MIM [33, 49]. The similarity between matching image pairs is optimized by minimizing a cross-entropy loss, while MIM is optionally performed. For adapting self-supervised learning frameworks to dense prediction tasks, objectives at the patch/region level are proposed to maximize the similarity between matching patches [2, 27, 42, 47]. However, the spatial sparsity interferes with the patch-level objective and turns the network pre-training unstable, as most event image patches, containing little to no events, provide meaningless supervision signals.

Event image self-supervised learning. Explorations of self-supervised learning on event data remain in an early stage. Existing works [46, 50] primarily leverage a pre-trained CLIP network [36] and paired RGB images for training, guiding the event network to have similar outputs with the RGB network (*i.e.*, the image encoder of CLIP) in feature space. Because an event image is more similar to its paired RGB image at a high-level than at a low-level [48], these approaches concentrate on capturing the overall structures of the event image. This explains their substantial performance improvements in object recognition tasks for event data while lagging in various dense prediction tasks. In this paper, we do not require paired RGB images and pre-trained RGB networks, and focus on pre-training a versatile network by utilizing solely event data for diverse dense prediction tasks on event datasets.

Event datasets. Event cameras are bio-inspired sensors that pixel-wisely record spatial location, time, and polarity of brightness changes in a scene as an event sequence. One of the largest-scale event datasets covering diverse scenes is the N-ImageNet dataset [26]. It is built by moving an event camera to observe RGB images (from the ImageNet-1K dataset [14]) rendered by a monitor, and inherits scene diversity from the ImageNet-1K dataset. Existing event image self-supervised learning frameworks favor leveraging the N-ImageNet dataset for pre-training, enabling transfer learning for tasks such as object recognition [11, 26, 34, 38], depth estimation [51], semantic segmentation [4, 20], and optical flow estimations [20, 51]. This paper focuses on pre-training a network for the above three dense prediction tasks. Moreover, considering the limited motion patterns in the N-ImageNet dataset [26], which are square, vertical, and horizontal, we curate a synthetic event dataset containing diverse motion patterns and scenes for pre-training.

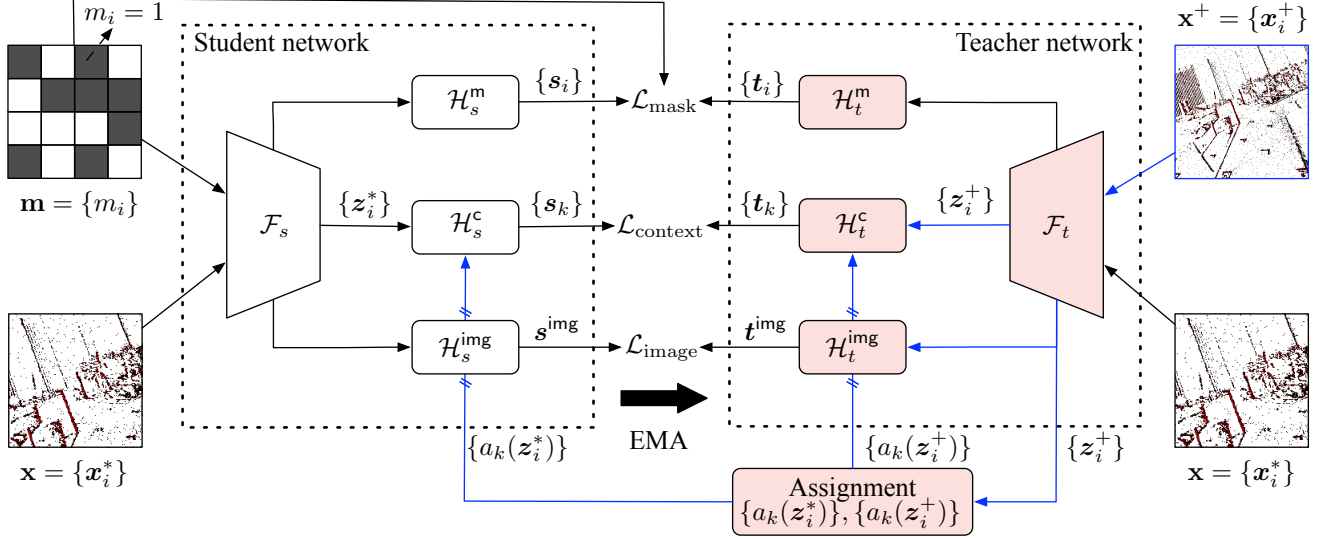


Figure 2. Overall architecture. During pre-training, our approach takes an event image \mathbf{x}^+ and its affine-transformed counterpart \mathbf{x}^* as inputs, producing a pre-trained backbone network \mathcal{F}_s . A teacher and student network are employed in the self-supervised training stage. Event images \mathbf{x}^+ and \mathbf{x}^* are tiled into N patches, denoted as $\mathbf{x}^+ = \{\mathbf{x}_i^+\}$ and $\mathbf{x}^* = \{\mathbf{x}_i^*\}$, $i = 1, \dots, N$. We randomly mask some patches of \mathbf{x}^* given to the student, but leave \mathbf{x}^* intact for the teacher. Patch-wise binary masks are represented by $\mathbf{m} = \{m_i\}$. Three similarity constraints are imposed based on output patch-wise features from the student and teacher backbones, respectively. They are: i) patch-level similarity. Patch-wise features of masked \mathbf{x}^* and \mathbf{x}^+ are separately projected by heads \mathcal{H}_s^m in the student network and \mathcal{H}_t^m in the teacher network, obtaining embeddings $\{s_i\}$ and $\{t_i\}$. To reconstruct masked patch embeddings, we employ a cross-entropy loss $\mathcal{L}_{\text{patch}}$. ii) context-level similarity. Features $\{z_i^+\}$ from the teacher network are assigned to K contexts, obtaining assignments $\{a_k(z_i^+)\}$. $a_k(z_i^+)$ denotes the membership of the feature z_i^+ to k -th context. The assignments of student features $\{z_i^*\}$ are computed by directly transferring $a_k(z_i^+)$ with an affine transformation. With the assignments $\{a_k(z_i^+)\}$ and $\{a_k(z_i^*)\}$, we collect and pool all features assigned to each context using modules \mathcal{H}_s^c and \mathcal{H}_t^c , generating context embeddings $\{s_k\}$ and $\{t_k\}$. A cross-entropy loss $\mathcal{L}_{\text{context}}$ is used to learn masked context embeddings; iii) image-level similarity. $\{z_i^*\}$ and $\{z_i^+\}$ are initially pooled separately and subsequently projected by the heads $\mathcal{H}_s^{\text{img}}$ and $\mathcal{H}_t^{\text{img}}$ into global image embeddings s^{img} and t^{img} . A cross-entropy loss $\mathcal{L}_{\text{image}}$ is used to encourage image-level similarity.

3. Method

We present our self-supervised method in this section. Our network is trained end-to-end, and the overall architecture is shown in Fig. 2.

Overall architecture. We aim to learn discriminative features from event data for dense prediction tasks, such as optical flow estimation. Sharing similarities with the learning process of DINOv2 [33], we convert raw events to an image [52], and construct two event images \mathbf{x}^+ and its augmentation \mathbf{x}^* . The two images are then fed into teacher and student networks to learn features, followed by enforcing similarities between the features of \mathbf{x}^+ and \mathbf{x}^* . We enforce three types of feature similarities: i) patch-level similarity; ii) context-level similarity; iii) image-level similarity. Details of our components are provided below.

Event image augmentations. We perform a 2D affine transformation on \mathbf{x}^+ , followed by GaussianBlur and ColorJitter [46], to create a distorted event image \mathbf{x}^* . We tile each image into N patches, i.e., $\mathbf{x}^+ = \{\mathbf{x}_i^+\}$ and $\mathbf{x}^* = \{\mathbf{x}_i^*\}$, $i = 1, \dots, N$. The linearity of the affine transformation establishes pixel correspondences between \mathbf{x}^+

and \mathbf{x}^* . For each pixel in \mathbf{x}^* , we can find its corresponding pixel in \mathbf{x}^+ , enabling context-level feature learning.

Image patches $\{\mathbf{x}_i^+\}$ and $\{\mathbf{x}_i^*\}$ are fed to the teacher and student networks for feature extraction. In the training stage, the student network is optimized by gradient descent. To avoid model collapse, the teacher network is kept as a momentum of the student network, and its parameters are updated with an exponential moving average (EMA) [24].

Patch-level similarity. We randomly mask some patches of \mathbf{x}^* given to the student, but leave \mathbf{x}^* intact for the teacher. The goal is to reconstruct masked patch embeddings, utilizing a cross-entropy loss between the patch features of both networks on each masked patch. This objective, introduced by [33], is briefly summarized below.

A patch-level binary mask $\mathbf{m} = \{m_i\}$, $i = 1, \dots, N$ is randomly sampled. For \mathbf{x}_i^* , it is masked and replaced by a [MASK] token if $m_i = 1$. The unmasked patches and [MASK] tokens are fed to the student network \mathcal{F}_s to extract features, and a feature projection head \mathcal{H}_s^m is employed to obtain patch embeddings $\{s_i\} = \mathcal{H}_s^m(\mathcal{F}_s(\mathbf{x}^*, \mathbf{m}))$.

Without masking, patches $\{\mathbf{x}_i^+\}$ are fed to the teacher network \mathcal{F}_t to extract features, followed by a feature pro-

jection head \mathcal{H}_t to extract patch embeddings $\{t_i\} = \mathcal{H}_t(\mathcal{F}_t(\mathbf{x}^*))$. The patch-level similarity objective is

$$\mathcal{L}_{\text{patch}} = \frac{1}{\|\mathbf{m}\|} \sum_{\substack{i=1 \\ m_i=1}}^N \text{CE}(t_i, s_i), \quad (1)$$

$$\text{CE}(t, s) = -\langle \mathcal{P}(t), \log \mathcal{P}(s) \rangle, \quad (2)$$

where $\|\cdot\|$ is the L1 norm that computes the number of masked patches. $\text{CE}(\cdot, \cdot)$ is the cross-entropy loss. $\mathcal{P}(\cdot)$ is the Softmax function that normalizes the patch embedding to a distribution. $\langle \cdot, \cdot \rangle$ is the dot product.

Context-level similarity. Reconstructing each masked patch embedding independently is prone to generating noisy embeddings. This is due to the sparsity of an event image. An event patch contains little information, and many patches are from a meaningless background (see Fig. 5). To overcome the limitations of independently reconstructing masked patch embeddings, we propose to mine contextual relationships among patch embeddings on the fly, and learn embeddings with context conditioning. We provide an overview in Fig. 3.

Specifically, we perform K-means clustering on patch features $\{z_i^+\} = \mathcal{F}_t(\mathbf{x}^+)$ of the teacher network, generating K cluster centers (i.e., contexts) and assignments $a_k(z_i^+)$. $a_k(z_i^+)$ denotes the membership of the feature z_i^+ to k -th context, i.e., it is 1 if z_i^+ is closest to k -th context and 0 otherwise.

For each context, features assigned to it are aggregated by an attention pooling network [36], generating a context embedding s_k . Collecting all context embeddings, we have embeddings $\{s_k\}, k = 1, \dots, K$, describing features $\mathcal{F}_t(\mathbf{x}^+)$ of the teacher network.

For patch features $\{z_i^*\} = \mathcal{F}_s(\mathbf{x}^*, \mathbf{m})$ of the student network, we use the same cluster centers. Due to the linearity of affine transformation, we can easily obtain the correspondence relationship between patches $\{x_i^*\}$ and $\{x_i^+\}$, and directly transfer the assignments $\{a_k(z_i^+)\}$ to get $\{a_k(z_i^*)\}$. Given assignments $a_k(z_i^*)$, we follow the same pipeline to aggregate features $\{z_i^*\}$ into context embeddings $\{t_k\}, k = 1, \dots, K$.

By using adaptively mined contexts, such as roads and buildings, as proxies, we overcome the sparsity limitation of enforcing event patch-level similarity. In essence, we aim to enforce the similarity between a group of patches belonging to the same context. The context-level similarity loss, denoted as $\mathcal{L}_{\text{context}}$, is defined below

$$\mathcal{L}_{\text{context}} = \frac{1}{K} \sum_{k=1}^K \text{CE}(t_k, s_k). \quad (3)$$

Image-level similarity. We aim to reconstruct masked image embedding of \mathbf{x}^* , by adding a cross-entropy loss be-

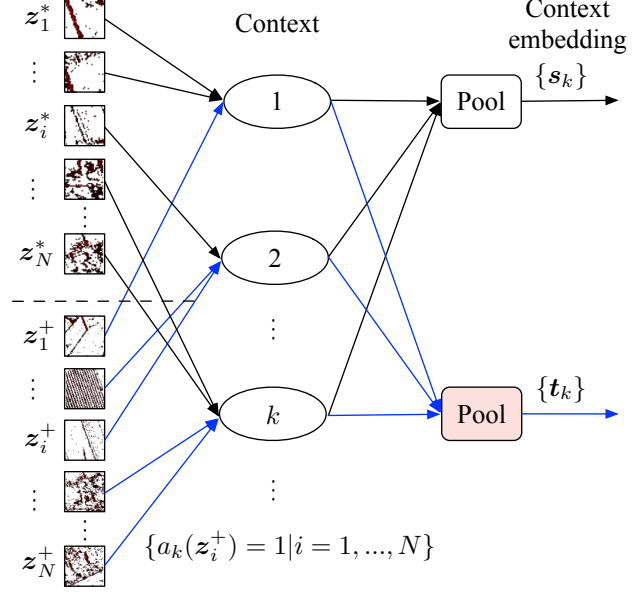


Figure 3. *Context assignment and aggregation.* Given patch-wise backbone features $\{z_i^*\}$ and $\{z_i^+\}$, we perform K-means clustering to mine K contexts, and obtain the patch-to-context assignments $\{a_k(z_i^*)\}$ and $\{a_k(z_i^+)\}$, respectively. For the k -th context, patch features $\{z_i^+\}$ assigned to it $\{a_k(z_i^+) = 1 | i = 1, \dots, N\}$ are pooled into a context embeddings t_k . Similarly, patch features $\{z_i^*\}$ are pooled into context embeddings $\{s_k\}$.

tween the image features of student and teacher networks on \mathbf{x}^* and \mathbf{x}^+ .

Patch features from the student and teacher network \mathcal{F}_s and \mathcal{F}_t are pooled and fed to feature projection heads $\mathcal{H}_s^{\text{img}}$ and $\mathcal{H}_t^{\text{img}}$, generating image-level feature embeddings s^{img} and t^{img} , respectively. The image-level similarity objective is given by

$$\mathcal{L}_{\text{image}} = \text{CE}(t^{\text{img}}, s^{\text{img}}). \quad (4)$$

Pre-training objective. Our network is trained end-to-end, and is optimized using the following objective:

$$\mathcal{L}_{\text{total}} = \mathcal{L}_{\text{mask}} + \lambda_1 \mathcal{L}_{\text{context}} + \lambda_2 \mathcal{L}_{\text{image}}. \quad (5)$$

where λ_1 and λ_2 are hyper-parameters for balancing losses.

4. Experiments

Pre-training dataset. To pre-train our network, we synthesize an E-TartanAir event camera dataset from the TartanAir dataset [41]. The TartanAir dataset is collected in photo-realistic simulation environments, featuring various light conditions, weather, and moving objects. It has 1037 sequences, with lengths ranging from 0.5K to 40K. The image resolution is 480×640 . In total, 180K training samples are generated. Details of the E-TartanAir synthesis process are given in the supplementary material.

Table 1. Comparison of semantic segmentation accuracies on the DDD17 [1, 4] and DSEC datasets [20, 39]. Mean interaction over union (mIoU (%)) and mean class accuracy (mACC (%)) are used as evaluation metrics.

Method	Backbone	Backbone Parameters	Pre-training Dataset	Pre-training Epochs	DDD17		DSEC	
					mIoU	mACC	mIoU	mACC
<i>Self-supervised ResNets.</i>								
SimCLR [7]	ResNet50	23M	ImageNet-1K	100	57.218	69.154	59.062	66.807
MoCo-v2 [9]	ResNet50	23M	ImageNet-1K	200	58.284	65.563	59.090	66.900
DenseCL [42]	ResNet50	23M	ImageNet-1K	200	57.969	71.840	59.121	68.935
ECDP [46]	ResNet50	23M	N-ImageNet	300	59.145	70.176	59.155	67.534
<i>Self-supervised Transformers.</i>								
MoCo-v3 [10]	ViT-S/16	21M	ImageNet-1K	300	53.654	68.122	49.211	57.133
BeiT [3]	ViT-B/16	86M	ImageNet-1K	800	52.391	61.950	46.524	55.068
IBoT [49]	ViT-S/16	21M	ImageNet-1K	800	49.940	57.916	42.532	50.617
MAE [25]	ViT-B/16	86M	ImageNet-1K	800	52.356	63.082	47.556	56.106
SelfPatch [47]	ViT-S/16	21M	ImageNet-1K	300	54.287	62.821	51.475	59.164
ESViT [27]	Swin-T/7	28M	ImageNet-1K	300	60.293	70.305	56.517	63.798
DINOv2 [33]	ViT-S/16	21M	LVD-142M	-	53.846	64.500	52.165	59.795
CIM [28]	ViT-B/16	86M	ImageNet-1K	300	54.013	63.926	51.582	59.628
ECDP [46]	ViT-S/16	21M	N-ImageNet	300	54.663	66.077	47.913	56.496
Ours	Swin-T/7	28M	E-TartanAir	300	62.525	74.301	61.250	69.620

Implementation details. We adopt the Swin Transformer [31] with the Swin-T/7 architecture as our backbone. The architectures of our projection heads follow [33, 36]. Our model is pre-trained for 300 epochs with batch size 1024. We set λ_1 and λ_2 to 0.9 and 0.1, respectively. An event image is tiled into 49 patches. The number of clusters is set to 8. Our pre-training framework is implemented in PyTorch, with additional details provided in the supplementary material. All codes and pre-trained models will be released.

Baselines. Our method is compared against two groups of methods: i) transfer learning of self-supervised pre-training. The initial weights of state-of-the-art methods are obtained in a self-supervised manner using the ImageNet-1K [14], N-ImageNet [26], or LVD-142M dataset [33]; ii) previous best. We compare with state-of-the-art methods specific to each downstream task, namely, semantic segmentation, flow estimation, and depth estimation.

4.1. Semantic Segmentation

Settings. Following the setup of [46], we evaluate on the standard DDD17 [1, 4] and DSEC dataset [20, 39] for semantic segmentation. The two datasets contain 19.8K and 5.4K samples, covering 6 and 11 semantic classes, respectively. Mean interaction over union (mIoU) and mean class accuracy (mAcc) are used as evaluation metrics.

Results. Tab. 1 gives the comparisons on the DDD17 and DSEC datasets. Our method achieves mIoU/mACC scores at 62.525%/74.301% and 61.250%/69.620% on the DDD17 and DSEC datasets, respectively, outperforming all others. Even though DINOv2 [33] is trained on the huge LVD-142M dataset, our method significantly outperforms it.

4.2. Flow Estimation

Settings. In accordance with [46], we compare our method with state-of-the-art methods on the MVSEC dataset [51]. End-point error (EPE) and outlier ratios (%) are used as evaluation metrics [40, 46].

Additionally, our method is also evaluated on the DSEC-Flow benchmark ¹[20, 21], securing the first-place position. A snapshot of the leaderboard is provided in the supplementary material.

Results. Tab. 2 presents the comparisons on ‘indoor_flying1’, ‘indoor_flying2’, and ‘indoor_flying3’ sequences of the MVSEC dataset. The EPE and outlier ratios of our method on the three sequences are 0.188/0.000, 0.578/1.188, and 0.472/0.196, respectively, significantly lower than all other methods.

Results for the DSEC-Flow benchmark are given in Tab. 3. Even compared with the unpublished method IDNet, previously holding the top position, our method achieves superior optical flow estimation accuracy.

4.3. Depth Estimation

Settings. We evaluate the performance of our methods for depth estimation on the MVSEC dataset [51]. Following [19], all methods are fine-tuned on the ‘outdoor_day2’ sequence. The evaluations are performed on the ‘outdoor_day1’, ‘outdoor_night1’, ‘outdoor_night2’, and ‘outdoor_night3’ sequences.

Results. Results are given in Tab. 4. Though the previous best method HMNet [23] performs supervised pre-training

¹<https://dsec.ifi.uzh.ch/uzh/dsec-flow-optical-flow-benchmark/>

Table 2. Comparison of optical flow estimation accuracies on the MVSEC dataset [51]. End-point error (EPE) and outlier ratios (%) [46] are used as evaluation metrics. Pixels with EPE above 3 and 5% of the ground truth optical flow magnitudes are deemed as outliers [32].

Method	Backbone	<i>indoor_flying1</i>		<i>indoor_flying2</i>		<i>indoor_flying3</i>	
		EPE	Outlier	EPE	Outlier	EPE	Outlier
<i>Self-supervised ResNets.</i>							
SimCLR [7]	ResNet50	0.646	0.488	1.445	9.331	1.188	5.507
MoCo-v2 [9]	ResNet50	0.612	0.459	1.359	8.683	1.130	5.201
ECDP [46]	ResNet50	0.604	0.354	1.352	8.572	1.122	5.263
DenseCL	ResNet50	0.634	0.529	1.349	7.596	1.130	5.176
<i>Self-supervised Transformers.</i>							
MoCo-v3 [10]	ViT-S/16	0.663	0.352	1.414	8.231	1.170	5.102
BeiT [3]	ViT-B/16	0.635	0.285	1.321	7.341	1.068	4.316
iBoT [49]	ViT-S/16	0.801	0.807	1.467	8.773	1.160	5.433
MAE [25]	ViT-B/16	0.613	0.167	1.293	6.952	1.109	4.635
SelfPatch [47]	ViT-S/16	0.623	0.317	1.337	7.894	1.097	5.286
ESViT [27]	Swin-T/7	0.812	1.224	1.338	8.316	1.078	5.185
DINOv2 [33]	ViT-S/16	0.602	0.325	1.196	6.185	0.990	4.333
CIM [28]	ViT-B/16	0.625	0.491	1.332	8.926	1.040	4.869
ECDP [46]	ViT-S/16	0.614	0.046	1.261	6.689	1.001	3.111
Ours	Swin-T/7	0.188	0.000	0.578	1.188	0.472	0.196

Table 3. Comparisons of optical flow estimation accuracies on the DSEC dataset [20]. Note that IDNet, ranking first previously, maintains anonymity. According to the DSEC leaderboard, we present results for 1/2/3-pixel error (1/2/3-PE), end-point error (EPE), and angular error (AE). All data in the table is sourced from the online benchmark.

Methods	1PE	2PE	3PE	EPE	AE
E-RAFT [21]	12.742	4.740	2.684	0.788	2.851
MultiCM [37]	76.570	48.480	30.855	3.472	13.983
E-Flowformer [29]	11.225	4.102	2.446	0.759	2.676
TMA [30]	10.863	3.972	2.301	0.743	2.684
OF_EV_SNN [13]	53.671	20.238	10.308	1.707	6.338
IDNet	10.069	3.497	2.036	0.719	2.723
Ours	8.887	3.199	1.958	0.697	2.575

using ground-truth depth before fine-tuning on the MVSEC dataset, our method still outperforms it. For example, the averaged root mean squared error across all sequences of our method and HMNet are 6.87 and 7.53, respectively.

Sample prediction results of our method on the semantic segmentation, optical flow estimation, and depth estimation tasks are provided in Fig. 4. Additional qualitative results can be found in the supplementary material.

4.4. Discussions

We perform ablations on the DSEC semantic segmentation dataset [20, 39] to study our model components.

Pre-training datasets. To study the effectiveness of our synthesized E-TartanAir dataset, we pre-train our method on different datasets. The results are given in Tab. 5a. Our method trained on the E-TartanAir dataset obtains the best performance. Furthermore, we pre-train state-of-the-art methods on the E-TartanAir dataset for comparisons, and results are given in Tab. 5b. Note that ESViT exhibits numerical instability during pre-training on the E-TartanAir

dataset. Our method gets the best performance.

Pre-training epochs. We explore the impact of pre-training epochs, ranging from 100 to 800, and the results are given in Fig. 6. Limited performance improvements are observed after 300 epochs, prompting us to set the pre-training epoch number to 300.

Context-level similarity. To check the effectiveness of our context-level similarity loss, we train several networks without using it, varying our backbone network and pre-training dataset. The results are given in Tab. 6. Results in Tab. 6 reveal that a network trained with $\mathcal{L}_{\text{context}}$ consistently outperforms its counterpart trained without using $\mathcal{L}_{\text{context}}$. For example, for networks trained on the E-tartanAir dataset with the Swin-T/7 backbone, without using $\mathcal{L}_{\text{context}}$, the mIOU/mACC scores are 55.556/63.486, which are lower than our best scores 61.250/69.620. This justifies the effectiveness of the proposed context-level similarity loss.

Sample results of patches belonging to different contexts are given in Fig. 5. Our method successfully mines contexts (tree, building, ground, and sky) in an event image,

Table 4. Comparison of depth estimation accuracies on the MVSEC dataset [51]. Threshold accuracy (δ_1 , δ_2 , and δ_3), absolute error (Abs), root mean squared error (RMS), and root mean squared logarithmic error (RMSlog) are used as evaluation metrics. Averaged scores across all sequences with and without a cutoff threshold at 30 meters are reported. The inputs of HMNet¹ are events, and HMNet² additionally takes RGB frames as inputs.

Method	Backbone	Average with cutoff threshold (≤ 30)						Average					
		δ_1	δ_2	δ_3	Abs	RMS	RMSlog	δ_1	δ_2	δ_3	Abs	RMS	RMSlog
<i>The best performance in the literature.</i>													
HMNet ¹ [23]	-	0.626	0.818	0.912	2.882	4.772	0.361	0.588	0.784	0.889	4.171	7.534	0.397
HMNet ² [23]	-	0.628	0.803	0.905	2.908	4.858	0.359	0.582	0.754	0.860	4.614	8.602	0.430
<i>Self-supervised ResNets.</i>													
SimCLR [7]	ResNet50	0.633	0.822	0.918	2.886	4.612	0.351	0.594	0.789	0.897	4.176	7.343	0.386
MoCo-v2 [9]	ResNet50	0.647	0.827	0.919	2.817	4.556	0.346	0.609	0.797	0.901	4.045	7.135	0.377
ECDP [46]	ResNet50	0.651	0.829	0.921	2.798	4.530	0.343	0.611	0.797	0.901	4.061	7.197	0.377
DenseCL [42]	ResNet50	0.649	0.826	0.920	2.813	4.541	0.344	0.610	0.798	0.903	4.036	7.121	0.375
<i>Self-supervised Transformers.</i>													
MoCo-v3 [10]	ViT-S/16	0.630	0.814	0.909	3.043	4.817	0.362	0.590	0.782	0.891	4.313	7.466	0.394
BeiT [3]	ViT-B/16	0.622	0.805	0.903	3.147	4.965	0.372	0.584	0.775	0.886	4.398	7.562	0.402
iBoT [49]	ViT-S/16	0.623	0.816	0.912	2.998	4.736	0.360	0.583	0.782	0.892	4.309	7.521	0.394
MAE [25]	ViT-B/16	0.612	0.802	0.900	3.214	5.075	0.377	0.575	0.772	0.884	4.449	7.601	0.405
SelfPatch [47]	ViT-S/16	0.605	0.801	0.900	3.435	5.067	0.380	0.567	0.768	0.882	4.515	7.735	0.410
ESViT [27]	Swin-T/7	0.644	0.829	0.923	2.796	4.482	0.342	0.604	0.796	0.903	4.083	7.219	0.377
DINOv2 [33]	ViT-S/16	0.612	0.805	0.903	3.181	5.030	0.375	0.575	0.774	0.885	4.449	7.653	0.406
CIM [28]	ViT-B/16	0.625	0.808	0.904	3.108	4.906	0.370	0.585	0.777	0.888	4.356	7.495	0.398
ECDP [46]	ViT-S/16	0.614	0.802	0.899	3.228	5.104	0.378	0.576	0.772	0.883	4.491	7.680	0.406
Ours	Swin-T/7	0.658	0.837	0.928	2.658	4.257	0.330	0.618	0.806	0.912	3.862	6.870	0.360

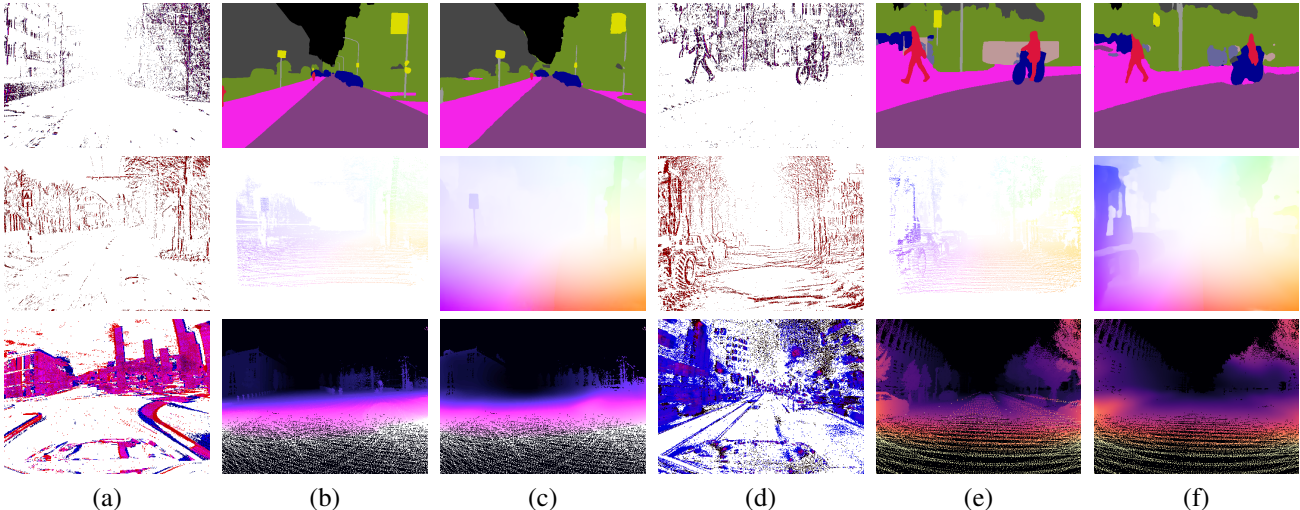


Figure 4. Qualitative results of dense predictions, namely, semantic segmentation (1st row), optical flow estimation (2nd row), and depth estimation (3rd row). (a) and (d): event images. Red and blue pixels depict positive and negative events, respectively. (b) and (e): ground-truth labels. (c) and (f): our model predictions. The brightness of images in the third row of (b) and (c) is enhanced to improve visualization.

and groups patches with the same semantics. Additional results are available in the supplementary material.

Number of contexts. Our model utilizes K context embeddings by aggregating patch features. To study the impact of contexts, we train our model with a different number of contexts. Results in Fig. 7 indicate that the best performance is achieved with 8 contexts. Increasing the number of contexts results in inferior performance. Due to the spar-

sity of event camera data, for large context numbers, many contexts aggregate features from event patches with little to no events. This results in noisy context embeddings, interferes with the training process, and hinders the network from learning discriminative event features.

Generalization ability of context-level similarity. To further demonstrate the effectiveness of the proposed $\mathcal{L}_{\text{context}}$, we add $\mathcal{L}_{\text{context}}$ to the objective function of the

Table 5. (a) Comparison of the performance of our method pre-trained on different datasets. (b) Comparison of state-of-the-art methods pre-trained on the E-TartanAir dataset.

(a) Pre-training datasets.			(b) Pre-training methods.				
Pre-training dataset	mIOU	mACC	Method	Backbone	Pre-training dataset	mIOU	ACC
DSEC	57.501	66.481	SelfPatch	Swin-T/7	E-TartanAir	57.243	66.070
DDD17	56.517	63.871	ESViT	Swin-T/7	E-TartanAir	24.630	31.248
N-imageNet	56.654	65.250	ECDP	Swin-T/7	E-TartanAir	56.568	64.234
E-TartanAir	61.250	69.620	Ours	Swin-T/7	E-TartanAir	61.250	69.620

Figure 5. Sample results of patches belonging to different contexts on the E-TartanAir dataset. (a): input event images. (b): mined context labels (without enforcing the context-level similarity). (c): mined context labels (enforcing the context-level similarity). (d) and (e): blends of the event image with context labels from (b) and (c) for visualization purposes, respectively

Table 6. Comparison of the performance of networks trained with and without using the proposed context-level similarity loss $\mathcal{L}_{context}$. Using $\mathcal{L}_{context}$ consistently improves accuracies.

Pre-training dataset	Backbone	Parameters	mIOU	mACC
$\mathcal{L}_{patch} + \mathcal{L}_{image}$				
N-ImageNet	ViT-S/16	21M	53.706	61.328
N-ImageNet	Swin-T/7	28M	54.905	63.271
E-TartanAir	ViT-S/16	21M	54.193	61.711
E-TartanAir	Swin-T/7	28M	55.556	63.486
$\mathcal{L}_{patch} + \mathcal{L}_{context} + \mathcal{L}_{image}$				
N-ImageNet	ViT-S/16	21M	54.897	62.527
N-ImageNet	Swin-T/7	28M	56.654	65.250
E-TartanAir	ViT-S/16	21M	55.729	64.771
E-TartanAir	Swin-T/7	28M	61.250	69.620

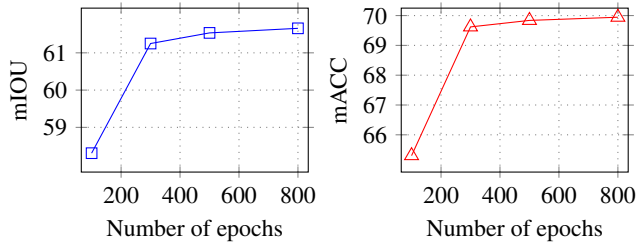


Figure 6. Comparison of the number of pre-training epochs.

state-of-the-art event data pre-training method, ECDP [46]. The mIOU/mAcc scores are increased from 47.913/56.496 to 53.826/61.008. The performance improvements validate the generalization ability of $\mathcal{L}_{context}$.

Limitation. Although our self-supervised pre-trained network has achieved state-of-the-art performance across vari-

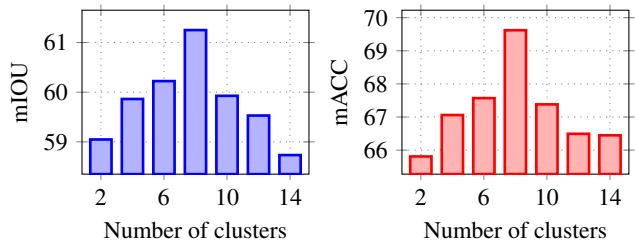


Figure 7. Comparison of the number of contexts.

ous dense prediction tasks, it necessitates task-specific fine-tuning to refine pre-trained network weights. However, we believe that our self-supervised learning exploration helps to learn task-agnostic pre-trained representations.

5. Conclusion and Broader Impact

We present a neural network trained for dense prediction tasks using an event camera. Our self-supervised learning method enforces three levels of similarity constraints: patch-level, context-level, and image-level. Our key insight is enforcing context similarity from event patch embeddings to pre-train our model. The proposed context-level similarity effectively addresses the sparsity problem of event data, resulting in state-of-the-art performance on semantic segmentation, optical flow, and depth estimation benchmarks. We believe that our dense pre-training techniques deserve a position in highly accurate event-based dense predictions.

Broader Impact. By aligning event data with paired RGB frames, our pre-training framework is promising to be extended to an event-vision-language foundation model. We hope it inspires future work.

References

- [1] Iñigo Alonso and Ana C. Murillo. Ev-segnet: Semantic segmentation for event-based cameras. In *IEEE Conference on Computer Vision and Pattern Recognition Workshops, CVPR Workshops 2019, Long Beach, CA, USA, June 16-20, 2019*, pages 1624–1633. Computer Vision Foundation / IEEE, 2019. [1](#), [5](#)
- [2] Yutong Bai, Xinlei Chen, Alexander Kirillov, Alan L. Yuille, and Alexander C. Berg. Point-level region contrast for object detection pre-training. In *IEEE/CVF Conference on Computer Vision and Pattern Recognition, CVPR 2022, New Orleans, LA, USA, June 18-24, 2022*, pages 16040–16049. IEEE, 2022. [2](#)
- [3] Hangbo Bao, Li Dong, Songhao Piao, and Furu Wei. Beit: BERT pre-training of image transformers. In *The Tenth International Conference on Learning Representations, ICLR 2022, Virtual Event, April 25-29, 2022*. OpenReview.net, 2022. [2](#), [5](#), [6](#), [7](#)
- [4] Jonathan Binas, Daniel Neil, Shih-Chii Liu, and Tobi Delbrück. DDD17: end-to-end DAVIS driving dataset. *CoRR*, abs/1711.01458, 2017. [1](#), [2](#), [5](#)
- [5] Mathilde Caron, Ishan Misra, Julien Mairal, Priya Goyal, Piotr Bojanowski, and Armand Joulin. Unsupervised learning of visual features by contrasting cluster assignments. In *Advances in Neural Information Processing Systems 33: Annual Conference on Neural Information Processing Systems 2020, NeurIPS 2020, December 6-12, 2020, virtual*, 2020. [2](#)
- [6] Mathilde Caron, Hugo Touvron, Ishan Misra, Hervé Jégou, Julien Mairal, Piotr Bojanowski, and Armand Joulin. Emerging properties in self-supervised vision transformers. In *2021 IEEE/CVF International Conference on Computer Vision, ICCV 2021, Montreal, QC, Canada, October 10-17, 2021*, pages 9630–9640. IEEE, 2021. [2](#)
- [7] Ting Chen, Simon Kornblith, Mohammad Norouzi, and Geoffrey E. Hinton. A simple framework for contrastive learning of visual representations. In *Proceedings of the 37th International Conference on Machine Learning, ICML 2020, 13-18 July 2020, Virtual Event*, pages 1597–1607. PMLR, 2020. [2](#), [5](#), [6](#), [7](#)
- [8] Xinlei Chen and Kaiming He. Exploring simple siamese representation learning. In *IEEE Conference on Computer Vision and Pattern Recognition, CVPR 2021, virtual, June 19-25, 2021*, pages 15750–15758. Computer Vision Foundation / IEEE, 2021. [2](#)
- [9] Xinlei Chen, Haoqi Fan, Ross Girshick, and Kaiming He. Improved baselines with momentum contrastive learning. *arXiv preprint arXiv:2003.04297*, 2020. [2](#), [5](#), [6](#), [7](#)
- [10] Xinlei Chen*, Saining Xie*, and Kaiming He. An empirical study of training self-supervised vision transformers. *arXiv preprint arXiv:2104.02057*, 2021. [2](#), [5](#), [6](#), [7](#)
- [11] Wensheng Cheng, Hao Luo, Wen Yang, Lei Yu, and Wei Li. Structure-aware network for lane marker extraction with dynamic vision sensor. *CoRR*, abs/2008.06204, 2020. [2](#)
- [12] Mehdi Cherti, Romain Beaumont, Ross Wightman, Mitchell Wortsman, Gabriel Ilharco, Cade Gordon, Christoph Schuhmann, Ludwig Schmidt, and Jenia Jitsev. Reproducible scaling laws for contrastive language-image learning. In *IEEE/CVF Conference on Computer Vision and Pattern Recognition, CVPR 2023, Vancouver, BC, Canada, June 17-24, 2023*, pages 2818–2829. IEEE, 2023. [1](#)
- [13] Javier Cuadrado, Ulysse Rancon, Benoit Cottureau, Francisco Barranco, and Timothée Masquelier. Optical flow estimation from event-based cameras and spiking neural networks. *Frontiers in Neuroscience*, 17, 2023. [6](#)
- [14] Jia Deng, Wei Dong, Richard Socher, Li-Jia Li, Kai Li, and Li Fei-Fei. Imagenet: A large-scale hierarchical image database. In *2009 IEEE Computer Society Conference on Computer Vision and Pattern Recognition (CVPR 2009), 20-25 June 2009, Miami, Florida, USA*, pages 248–255. IEEE Computer Society, 2009. [2](#), [5](#)
- [15] Alexey Dosovitskiy, Lucas Beyer, Alexander Kolesnikov, Dirk Weissenborn, Xiaohua Zhai, Thomas Unterthiner, Mostafa Dehghani, Matthias Minderer, Georg Heigold, Sylvain Gelly, Jakob Uszkoreit, and Neil Houlsby. An image is worth 16x16 words: Transformers for image recognition at scale. In *9th International Conference on Learning Representations, ICLR 2021, Virtual Event, Austria, May 3-7, 2021*. OpenReview.net, 2021. [1](#)
- [16] Patrick Esser, Robin Rombach, and Björn Ommer. Taming transformers for high-resolution image synthesis. In *IEEE Conference on Computer Vision and Pattern Recognition, CVPR 2021, virtual, June 19-25, 2021*, pages 12873–12883. Computer Vision Foundation / IEEE, 2021. [2](#)
- [17] Yuxin Fang, Wen Wang, Binhui Xie, Quan Sun, Ledell Wu, Xinggang Wang, Tiejun Huang, Xinlong Wang, and Yue Cao. EVA: exploring the limits of masked visual representation learning at scale. In *IEEE/CVF Conference on Computer Vision and Pattern Recognition, CVPR 2023, Vancouver, BC, Canada, June 17-24, 2023*, pages 19358–19369. IEEE, 2023. [2](#)
- [18] Guillermo Gallego, Tobi Delbrück, Garrick Orchard, Chiara Bartolozzi, Brian Taba, Andrea Censi, Stefan Leutenegger, Andrew J. Davison, Jörg Conradt, Kostas Daniilidis, and Davide Scaramuzza. Event-based vision: A survey. *IEEE Trans. Pattern Anal. Mach. Intell.*, 44(1):154–180, 2022. [1](#)
- [19] Daniel Gehrig, Michelle Rüegg, Mathias Gehrig, Javier Hidalgo-Carrió, and Davide Scaramuzza. Combining events and frames using recurrent asynchronous multimodal networks for monocular depth prediction. *IEEE Robotics Autom. Lett.*, 6(2):2822–2829, 2021. [5](#)
- [20] Mathias Gehrig, Willem Aarents, Daniel Gehrig, and Davide Scaramuzza. DSEC: A stereo event camera dataset for driving scenarios. *IEEE Robotics Autom. Lett.*, 6(3):4947–4954, 2021. [1](#), [2](#), [5](#), [6](#)
- [21] Mathias Gehrig, Mario Millhäusler, Daniel Gehrig, and Davide Scaramuzza. E-RAFT: dense optical flow from event cameras. In *International Conference on 3D Vision, 3DV 2021, London, United Kingdom, December 1-3, 2021*, pages 197–206. IEEE, 2021. [1](#), [2](#), [5](#), [6](#)
- [22] Jean-Bastien Grill, Florian Strub, Florent Altché, Corentin Tallec, Pierre H. Richemond, Elena Buchatskaya, Carl Doersch, Bernardo Ávila Pires, Zhaohan Guo, Mohammad Gheshlaghi Azar, Bilal Piot, Koray Kavukcuoglu, Rémi Munos, and Michal Valko. Bootstrap your own latent - A

- new approach to self-supervised learning. In *Advances in Neural Information Processing Systems 33: Annual Conference on Neural Information Processing Systems 2020, NeurIPS 2020, December 6-12, 2020, virtual*, 2020. [2](#)
- [23] Ryuhei Hamaguchi, Yasutaka Furukawa, Masaki Onishi, and Ken Sakurada. Hierarchical neural memory network for low latency event processing. In *IEEE/CVF Conference on Computer Vision and Pattern Recognition, CVPR 2023, Vancouver, BC, Canada, June 17-24, 2023*, pages 22867–22876. IEEE, 2023. [1](#), [5](#), [7](#)
- [24] Kaiming He, Haoqi Fan, Yuxin Wu, Saining Xie, and Ross B. Girshick. Momentum contrast for unsupervised visual representation learning. In *2020 IEEE/CVF Conference on Computer Vision and Pattern Recognition, CVPR 2020, Seattle, WA, USA, June 13-19, 2020*, pages 9726–9735. Computer Vision Foundation / IEEE, 2020. [2](#), [3](#)
- [25] Kaiming He, Xinlei Chen, Saining Xie, Yanghao Li, Piotr Dollár, and Ross B. Girshick. Masked autoencoders are scalable vision learners. In *IEEE/CVF Conference on Computer Vision and Pattern Recognition, CVPR 2022, New Orleans, LA, USA, June 18-24, 2022*, pages 15979–15988. IEEE, 2022. [2](#), [5](#), [6](#), [7](#)
- [26] Junho Kim, Jaehyeok Bae, Gangin Park, Dongsu Zhang, and Young Min Kim. N-imagenet: Towards robust, fine-grained object recognition with event cameras. In *Proceedings of the IEEE/CVF International Conference on Computer Vision (ICCV)*, pages 2146–2156, 2021. [2](#), [5](#)
- [27] Chunyuan Li, Jianwei Yang, Pengchuan Zhang, Mei Gao, Bin Xiao, Xiyang Dai, Lu Yuan, and Jianfeng Gao. Efficient self-supervised vision transformers for representation learning. In *The Tenth International Conference on Learning Representations, ICLR 2022, Virtual Event, April 25-29, 2022*. OpenReview.net, 2022. [1](#), [2](#), [5](#), [6](#), [7](#)
- [28] Wei Li, Jiahao Xie, and Chen Change Loy. Correlational image modeling for self-supervised visual pre-training. In *IEEE/CVF Conference on Computer Vision and Pattern Recognition, CVPR 2023, Vancouver, BC, Canada, June 17-24, 2023*, pages 15105–15115. IEEE, 2023. [5](#), [6](#), [7](#)
- [29] Yijin Li, Zhaoyang Huang, Shuo Chen, Xiaoyu Shi, Hongsheng Li, Hujun Bao, Zhaopeng Cui, and Guofeng Zhang. Blinkflow: A dataset to push the limits of event-based optical flow estimation. *CoRR*, abs/2303.07716, 2023. [6](#)
- [30] Haotian Liu, Guang Chen, Sanqing Qu, Yanping Zhang, Zhijun Li, Alois Knoll, and Changjun Jiang. Tma: Temporal motion aggregation for event-based optical flow. In *ICCV*, 2023. [6](#)
- [31] Ze Liu, Yutong Lin, Yue Cao, Han Hu, Yixuan Wei, Zheng Zhang, Stephen Lin, and Baining Guo. Swin transformer: Hierarchical vision transformer using shifted windows. In *2021 IEEE/CVF International Conference on Computer Vision, ICCV 2021, Montreal, QC, Canada, October 10-17, 2021*, pages 9992–10002. IEEE, 2021. [5](#)
- [32] M. Menze, Christian Heipke, and Andreas Geiger. Joint 3d estimation of vehicles and scene flow. *ISPRS Annals of Photogrammetry, Remote Sensing and Spatial Information Sciences*, II-3/W5:427–434, 2015. [6](#)
- [33] Maxime Oquab, Timothée Darcet, Théo Moutakanni, Huy Vo, Marc Szafraniec, Vasil Khalidov, Pierre Fernandez, Daniel Haziza, Francisco Massa, Alaaeldin El-Nouby, Mahmoud Assran, Nicolas Ballas, Wojciech Galuba, Russell Howes, Po-Yao Huang, Shang-Wen Li, Ishan Misra, Michael G. Rabbat, Vasu Sharma, Gabriel Synnaeve, Hu Xu, Hervé Jégou, Julien Mairal, Patrick Labatut, Armand Joulin, and Piotr Bojanowski. Dinov2: Learning robust visual features without supervision. *CoRR*, abs/2304.07193, 2023. [2](#), [3](#), [5](#), [6](#), [7](#)
- [34] Garrick Orchard, Ajinkya Jayawant, Gregory Cohen, and Nitish V. Thakor. Converting static image datasets to spiking neuromorphic datasets using saccades. *CoRR*, abs/1507.07629, 2015. [2](#)
- [35] Zhiliang Peng, Li Dong, Hangbo Bao, Qixiang Ye, and Furu Wei. Beit v2: Masked image modeling with vector-quantized visual tokenizers. *CoRR*, abs/2208.06366, 2022. [2](#)
- [36] Alec Radford, Jong Wook Kim, Chris Hallacy, Aditya Ramesh, Gabriel Goh, Sandhini Agarwal, Girish Sastry, Amanda Askell, Pamela Mishkin, Jack Clark, Gretchen Krueger, and Ilya Sutskever. Learning transferable visual models from natural language supervision. In *Proceedings of the 38th International Conference on Machine Learning, ICML 2021, 18-24 July 2021, Virtual Event*, pages 8748–8763. PMLR, 2021. [2](#), [4](#), [5](#)
- [37] Shintaro Shiba, Yoshimitsu Aoki, and Guillermo Gallego. Secrets of event-based optical flow. In *Computer Vision - ECCV 2022 - 17th European Conference, Tel Aviv, Israel, October 23-27, 2022, Proceedings, Part XVIII*, pages 628–645. Springer, 2022. [6](#)
- [38] Amos Sironi, Manuele Brambilla, Nicolas Bourdis, Xavier Lagorce, and Ryad Benosman. HATS: histograms of averaged time surfaces for robust event-based object classification. In *2018 IEEE Conference on Computer Vision and Pattern Recognition, CVPR 2018, Salt Lake City, UT, USA, June 18-22, 2018*, pages 1731–1740. Computer Vision Foundation / IEEE Computer Society, 2018. [2](#)
- [39] Zhaoning Sun, Nico Messikommer, Daniel Gehrig, and Davide Scaramuzza. ESS: learning event-based semantic segmentation from still images. In *Computer Vision - ECCV 2022 - 17th European Conference, Tel Aviv, Israel, October 23-27, 2022, Proceedings, Part XXXIV*, pages 341–357. Springer, 2022. [1](#), [5](#), [6](#)
- [40] Zhexiong Wan, Yuchao Dai, and Yuxin Mao. Learning dense and continuous optical flow from an event camera. *IEEE Trans. Image Process.*, 31:7237–7251, 2022. [5](#)
- [41] Wenshan Wang, Delong Zhu, Xiangwei Wang, Yaoyu Hu, Yuheng Qiu, Chen Wang, Yafei Hu, Ashish Kapoor, and Sebastian A. Scherer. Tartanair: A dataset to push the limits of visual SLAM. In *IEEE/RSJ International Conference on Intelligent Robots and Systems, IROS 2020, Las Vegas, NV, USA, October 24, 2020 - January 24, 2021*, pages 4909–4916. IEEE, 2020. [2](#), [4](#)
- [42] Xinlong Wang, Rufeng Zhang, Chunhua Shen, Tao Kong, and Lei Li. Dense contrastive learning for self-supervised visual pre-training. In *IEEE Conference on Computer Vision and Pattern Recognition, CVPR 2021, virtual, June 19-25, 2021*, pages 3024–3033. Computer Vision Foundation / IEEE, 2021. [1](#), [2](#), [5](#), [7](#)

- [43] David Weikersdorfer, David B. Adrian, Daniel Cremers, and Jörg Conradt. Event-based 3d SLAM with a depth-augmented dynamic vision sensor. In *2014 IEEE International Conference on Robotics and Automation, ICRA 2014, Hong Kong, China, May 31 - June 7, 2014*, pages 359–364. IEEE, 2014. [1](#)
- [44] Zhirong Wu, Yuanjun Xiong, Stella X. Yu, and Dahua Lin. Unsupervised feature learning via non-parametric instance discrimination. In *2018 IEEE Conference on Computer Vision and Pattern Recognition, CVPR 2018, Salt Lake City, UT, USA, June 18-22, 2018*, pages 3733–3742. Computer Vision Foundation / IEEE Computer Society, 2018. [2](#)
- [45] Zhenda Xie, Zheng Zhang, Yue Cao, Yutong Lin, Jianmin Bao, Zhuliang Yao, Qi Dai, and Han Hu. Simmim: a simple framework for masked image modeling. In *IEEE/CVF Conference on Computer Vision and Pattern Recognition, CVPR 2022, New Orleans, LA, USA, June 18-24, 2022*, pages 9643–9653. IEEE, 2022. [2](#)
- [46] Yan Yang, Liyuan Pan, and Liu Liu. Event camera data pre-training. In *Proceedings of the IEEE/CVF International Conference on Computer Vision (ICCV)*, pages 10699–10709, 2023. [1](#), [2](#), [3](#), [5](#), [6](#), [7](#), [8](#)
- [47] Sukmin Yun, Hankook Lee, Jaehyung Kim, and Jinwoo Shin. Patch-level representation learning for self-supervised vision transformers. In *IEEE/CVF Conference on Computer Vision and Pattern Recognition, CVPR 2022, New Orleans, LA, USA, June 18-24, 2022*, pages 8344–8353. IEEE, 2022. [2](#), [5](#), [6](#), [7](#)
- [48] Dehao Zhang, Qiankun Ding, Peiqi Duan, Chu Zhou, and Boxin Shi. Data association between event streams and intensity frames under diverse baselines. In *Computer Vision - ECCV 2022 - 17th European Conference, Tel Aviv, Israel, October 23-27, 2022, Proceedings, Part VII*, pages 72–90. Springer, 2022. [2](#)
- [49] Jinghao Zhou, Chen Wei, Huiyu Wang, Wei Shen, Cihang Xie, Alan L. Yuille, and Tao Kong. Image BERT pre-training with online tokenizer. In *The Tenth International Conference on Learning Representations, ICLR 2022, Virtual Event, April 25-29, 2022*. OpenReview.net, 2022. [2](#), [5](#), [6](#), [7](#)
- [50] Jiazhou Zhou, Xu Zheng, Yuanhuiyi Lyu, and Lin Wang. E-CLIP: towards label-efficient event-based open-world understanding by CLIP. *CoRR*, abs/2308.03135, 2023. [1](#), [2](#)
- [51] Alex Zihao Zhu, Dinesh Thakur, Tolga Özaslan, Bernd Pfrommer, Vijay Kumar, and Kostas Daniilidis. The multi vehicle stereo event camera dataset: An event camera dataset for 3d perception. *CoRR*, abs/1801.10202, 2018. [1](#), [2](#), [5](#), [6](#), [7](#)
- [52] Alex Zihao Zhu, Liangzhe Yuan, Kenneth Chaney, and Kostas Daniilidis. Unsupervised event-based learning of optical flow, depth, and egomotion. *CoRR*, abs/1812.08156, 2018. [3](#)